GREENSUSMATER

Greensusmater
Vol. 1, No. 1, March 2024
https://doi.org/10.62755/greensusmater.2024.1.1.9-14

Effect of calcination temperature on the performance of hydrothermally grown cerium dioxide (CeO_2) nanorods for the removal of Congo red dyes

Aditya Rianjanu[1,2], Resti Nuraeni[1] Rizky Aflaha[3], Nur Istiqomah Khamidy[1], Kuwat Triyana[3], Tarmizi Taher[2,4]

[1] *Department of Materials Engineering, Institut Teknologi Sumatera, Terusan Ryacudu, Way Hui, Jati Agung, Lampung Selatan 35365, Indonesia*
[2] *Center for Green and Sustainable Materials, Institut Teknologi Sumatera, Terusan Ryacudu, Way Hui, Jati Agung, Lampung Selatan 35365, Indonesia*
[3] *Department of Physics, Faculty of Mathematics and Natural Sciences, Universitas Gadjah Mada, Sekip Utara PO Box BLS 21, Yogyakarta 55281, Indonesia*
[4] *Department of Environmental Engineering, Institut Teknologi Sumatera, Terusan Ryacudu, Way Hui, Jati Agung, Lampung Selatan 35365, Indonesia*

Corresponding author: aditya.rianjanu@mt.itera.ac.id. (AR), tarmizi.taher@tl.itera.ac.id (TT)

ARTICLE HISTORY: Received: January 30, 2024 | Revised: February 18, 2024 | Accepted: February 20, 2024

ABSTRACT

This study investigates the transformation of CeO_2 nanostructures through various calcination temperatures and their subsequent impact on morphological, structural, and photocatalytic properties. X-ray diffraction (XRD) analysis reveals the presence of cerium oxycarbonate in the uncalcined samples, transitioning to a face-centered cubic CeO_2 phase post-calcination at 500 °C. The scanning electron microscopy (SEM) imaging delineates a morphological evolution from distinct, rod-like structures in the uncalcined state to sintered, agglomerated forms as calcination temperatures ascend from 500 °C to 800 °C. The crystallite size, calculated using Scherrer's Equation, displayed a proportional increase with temperature. The photocatalytic degradation of Congo red dye under UV light was analyzed using UV-Vis spectroscopy, with the calcined samples exhibiting varying degrees of adsorption and photocatalytic activity. The study found that higher calcination temperatures correlate with increased photocatalytic performance, potentially due to enhanced crystallinity. This assertion is supported by pseudo-first-order kinetic modeling, indicating improved photocatalytic efficiency with higher calcination temperatures, underlined by increasing rate constants. These findings underscore the intricate relationship between calcination-induced morphological and structural changes and the photocatalytic prowess of CeO_2 nanostructures.

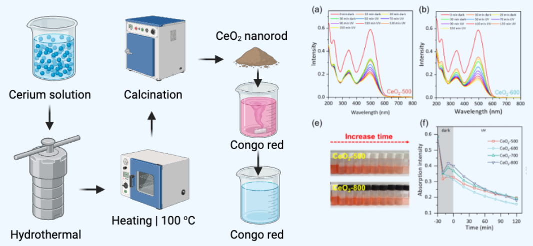

Keywords: *Rare-earth Metal Oxide; Adsorption; Degradation; Wastewater Treatment; Cerium Oxide*

1. INTRODUCTION

Photocatalytic degradation has emerged as a compelling method to tackle the issue of dye pollution in wastewater treatment, due to its potential for complete mineralization of organic pollutants into non-toxic byproducts [1, 2, 3]. Several semiconductors, such as ZnO, TiO_2, SnO_2, MnO_2, Fe_2O_3, NiO, WO_3, Nb_2O_5, and CeO_2, have been developed as effective photocatalytic materials [4, 5, 6, 7, 8]. Cerium dioxide (CeO_2), in particular, has garnered increasing attention in the field of environmental engineering for its remarkable redox properties, high oxygen storage capacity, and stability [9, 10]. These attributes render it an indispensable material for applications in catalysis, fuel cells, and as an additive in diesel fuels to reduce emissions [11]. Recent advancements in nanotechnology have further enhanced the utility of CeO_2, especially in nanostructured forms, which exhibit unique properties attributable to their high surface-to-volume ratio and quantum size effects [12]. These nanostructures are typically synthesized using various methods, with the hydrothermal process being one of the most favored due to its relatively mild conditions, scalability, and the quality of the resultant products [13, 14]. The resultant morphologies, including rod-like structures, are often determined by the synthetic conditions and can be fine-tuned to optimize the material's performance for specific applications.

Our previous study highlighted the potential application of CeO_2 nanorods, fabricated using the hydrothermal process, as photocatalysts in dye degradation [15]. However, their performance needs enhancement to produce high-performance photocatalytic materials. Literature suggests that increasing the calcination temperature leads to materials with better photocatalytic performance [16]. The calcination process plays a pivotal role in tailoring the properties of metal oxide nanostructures. It is known to induce morphological changes, enhance crystallinity, and remove organic residues or other volatile contaminants [17, 18]. These alterations are crucial as they directly influence the material's catalytic activity, adsorptive capacities, and overall chemical reactivity. Calcination temperature is a critical parameter; it can dictate the phase stability and surface characteristics of the resulting CeO_2. While lower temperatures may be sufficient to induce phase changes from precursors such as cerium oxycarbonate to pure CeO_2, higher temperatures may lead to sintering, growth of crystallite size, and potentially the formation of secondary phases. This study aims to understand the relation-

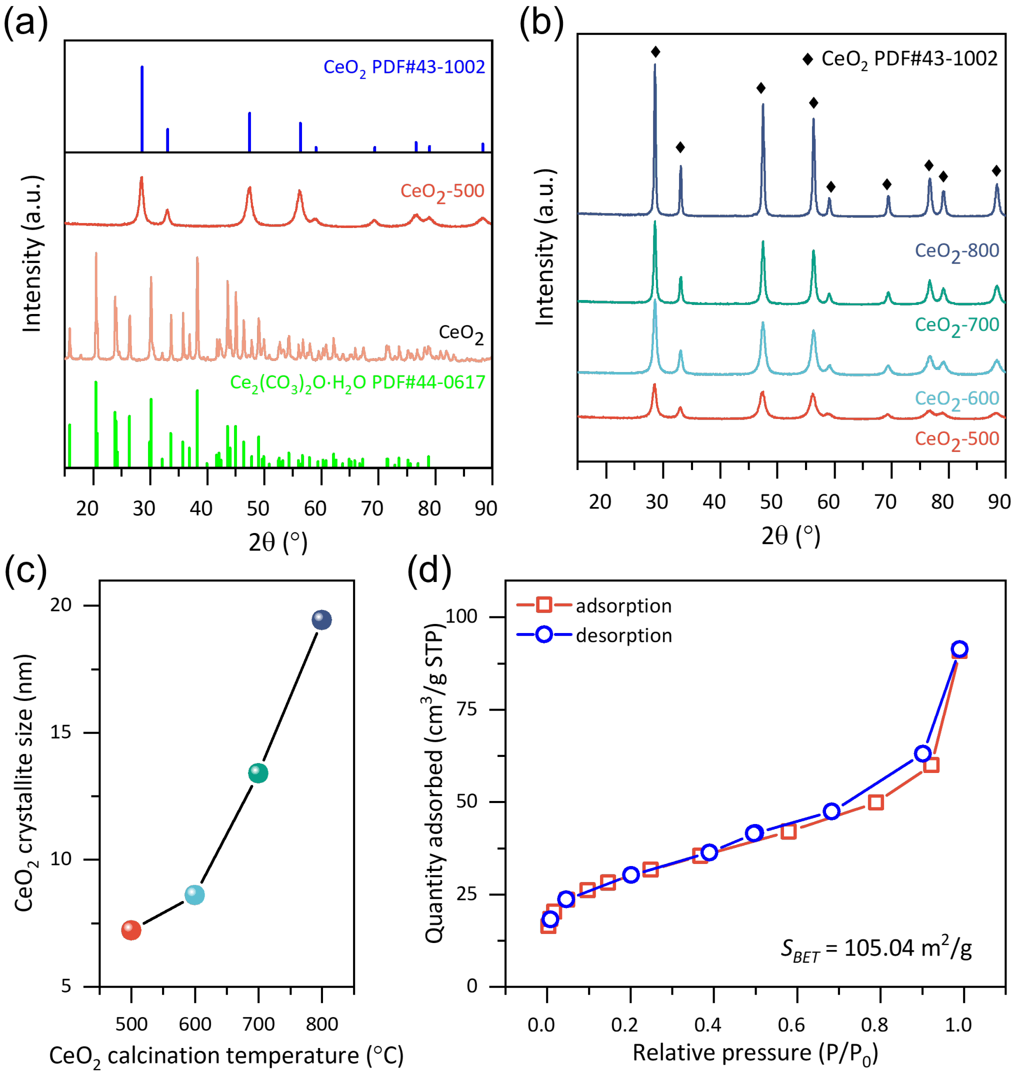

Figure 1. The XRD pattern of (a) calcined (CeO_2-500) vs uncalcined CeO_2 and (b) CeO_2 calcined at different temperature. (c) The CeO_2 crystallite size calculated from XRD patterns. (d) BET analysis of the CeO_2-500 samples.

ship between calcination conditions and the characteristics of the resulting CeO_2 nanostructures, which is essential for optimizing their performance in environmental applications.

2. EXPERIMENTAL SECTION

2.1 Materials

Cerium nitrate hexahydrate ($Ce(NO_3)_3 \cdot 6\,H_2O$), urea ($CO(NH_2)_2$), and Congo red (CR, C.I. 22120) were purchased from Merck, Darmstadt, Germany. The deionized (DI) water was used as solvent both during the hydrothermal and dye degradation measurements. All materials were used as received without any further purifications.

2.2 Preparation of CeO_2 nanostructures and materials characterizations

The CeO_2 nanorods were fabricated similar to our previously reported study [15]. Typically, 3.0 g of $Ce(NO_3)_3$ and 4.2 g of $CO(NH_2)_2$ were dissolved in 70 mL deionized water using a magnetic stirrer until the salt completely dissolved. The mixed solution was then placed inside a 100-mL Teflon-lined autoclave and sealed tightly for the hydrothermal process. The hydrothermal growth took place at a temperature of 100 °C for 12 hours inside an electric oven. The solid was then washed with DI water and filtered several times using a vacuum filter. The solid powder was dried in an electric oven at 80 °C for 4 hours before calcination. To investigate the effect of calcination temperature on the dye removal performance, the calcination temperatures were varied (i.e., 500, 600, 700, and 800 °C) and the samples were named CeO_2-500, CeO_2-600, CeO_2-700, and CeO_2-800, respectively. Each sample was calcined using a predetermined holding temperature and held for 2 hours, with a ramp of 5 °C/min. A yellowish powder was obtained for each calcination temperature and used for materials characterization and dye removal investigations. To investigate the effect of the calcination temperature on the CeO_2 morphology and crystalline structure, scanning electron microscopy (SEM, JEOL JSM-6510) and X-ray diffractometry (XRD, BRUKER D8 ADVANCE ECO) were used respectively.

2.3 Photocatalytic dye degradation measurements

For the photodegradation investigation, we used a photoreactor chamber equipped with four Phillips UVC lamps (10 W, $\lambda \approx 253.7$ nm). Congo red (CR) aqueous solution was

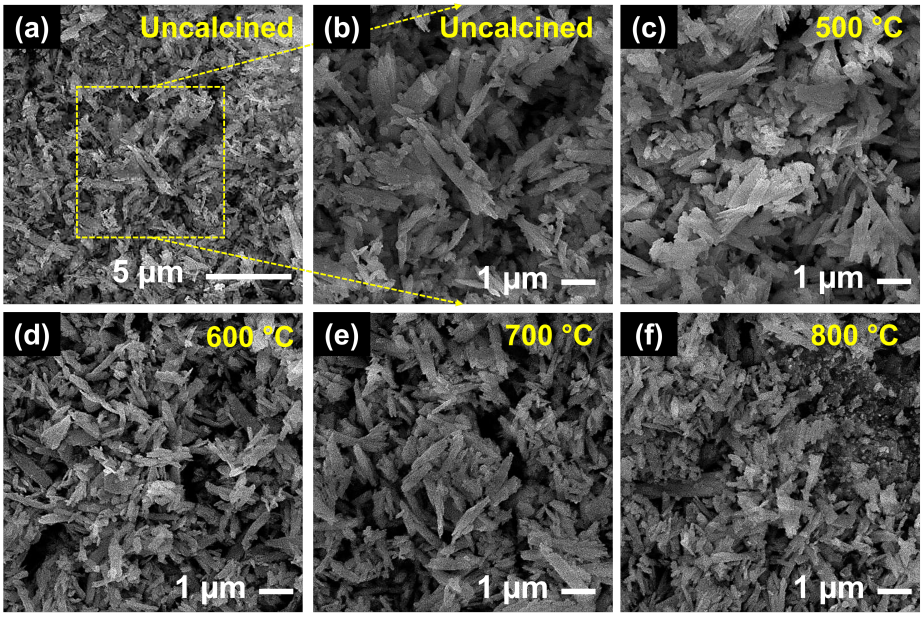

Figure 2. The SEM images of the (a) uncalcined CeO_2, and calcined CeO_2 (b) CeO_2-500, (d) CeO_2-600, (e) CeO_2-700, and (f) CeO_2-800 samples

prepared with a concentration of 10 ppm as the model dye. Typically, 50 mg of CeO_2 powder was put into 100 mL CR solutions (10 ppm) and stirred inside the photoreactor chamber. The reaction was initially taken place under dark conditions for 30 min to achieve stable adsorption conditions. After that, the UV lamp was then turned on, and the CR solution was subjected to UV irradiations. Every 20 min, 3.5 mL suspension was taken and filtered using polyvinylidene fluoride (PVDF) syringe filters to separate the CeO_2 powder. The absorption spectra of 3.5 mL of each time variation were then measured by a UV-Vis spectrophotometer (Shimadzu UV-1280). The measurement was done for all samples (CeO_2-500, CeO_2-600, CeO_2-700, and CeO_2-800). The concentration of the CR solutions was determined using the absorbance value at the maximum wavelength ($\lambda = 498$ nm).

3. RESULTS AND DISCUSSION

Figure 1 shows the XRD pattern of the uncalcined and calcined CeO_2 samples. The uncalcined CeO_2 samples show characteristics of cerium oxycarbonate ($Ce_2(CO_3)_2O \cdot H_2O$) in accordance with the PDF number 44-0617 (Figure 1a), which is similar to previous literatures [19]. This phase is a well-known oxycarbonate of cerium that is mostly obtained through precipitation of cerium salt through hydrolysis of urea [20]. After calcination (CeO_2-500), a new crystal phase was obtained, which has excellent similarity with the XRD pattern of face-centered cubic (FCC) CeO_2 (PDF#43-1002) [21, 22]. Previous studies found that the organic residues obtained during the hydrothermal process of CeO_2 start to decompose at a temperature of 320 °C [23, 24]. Based on that information, we believed that a calcination temperature of 500 °C is sufficient to convert cerium oxycarbonate into face-centered cubic CeO_2 [25]. The peaks were observed at 2θ values of 28.5°; 33.1°; 47.5°; 56.3°; 59.1°; 69.4°; 76.7°; 79.1°; and 88.4°, which correspond to the (hkl) planes of (111), (200), (220), (311), (222), (400), (331), (420), and (422), respectively.

The influence of various calcination temperatures on the crystalline phase of CeO_2 is depicted in Figure 1b. Characteristic peaks of face-centered cubic (FCC) CeO_2 were observed for all samples, without the presence of additional or secondary cerium phases, confirming the successful fabrication of CeO_2 nanostructures. Furthermore, the peak intensity and sharpness corresponding to cubic CeO_2 increased with the calcination temperature. Figure 1c presents the crystallite sizes of the CeO_2 samples at different calcination temperatures, calculated from the XRD data using Scherrer's Equation [26, 27]. The crystallite size was calculated to be 7.2 nm, 8.6 nm, 13.4 nm, and 19.4 nm for the CeO_2-500, CeO_2-600, CeO_2-700, and CeO_2-800, respectively. The crystallite size increases with increasing calcination temperature. These findings are consistent with previously reported studies [28, 29]. We also performed the nitrogen (N_2) adsorption-desorption isotherm using surface area analyzer (Quantachrome QuadraWin ©2000-16). The quantity adsorbed during adsorption/desorption process with various relative pressure were shown in Figure 1d. It shows type IV hysteresis loop revealing the existence of mesopore similar to previous literatures [30, 31, 32] . Moreover, the BET (Brunauer, Emmett and Teller) surface area (SBET) of the CeO2-500 shows a remarkable value of 105.04 m^2/g, implying that the material has high surface area.

Figure 2 showcases the SEM images of (a,b) uncalcined CeO_2, and calcined CeO_2 at (c) CeO_2-500, (d) CeO_2-600, (e) CeO_2-700, and (f) CeO_2-800. The morphological effects of calcination temperature on CeO_2 nanostructures were also investigated using the SEM images featured in Figure 2. Images of the CeO_2 sample without calcination treatment (Figure 2a and 2b) show that the CeO_2 has formed into elongated, rod-like structures with a relatively uniform size and orientation, indicative of the typical morphology of CeO_2 fabricated via the hydrothermal process [15, 33]. A similar morphology was also observed for the CeO_2 sample after calcinations. For example, the CeO_2-500 (Figure 2c) also shows a relatively uniform rod-like structure. However, as the calcination temperature were increasing for CeO_2-600 to CeO_2-800 samples in which shown in Figure 2d to 2f a more distinctive different

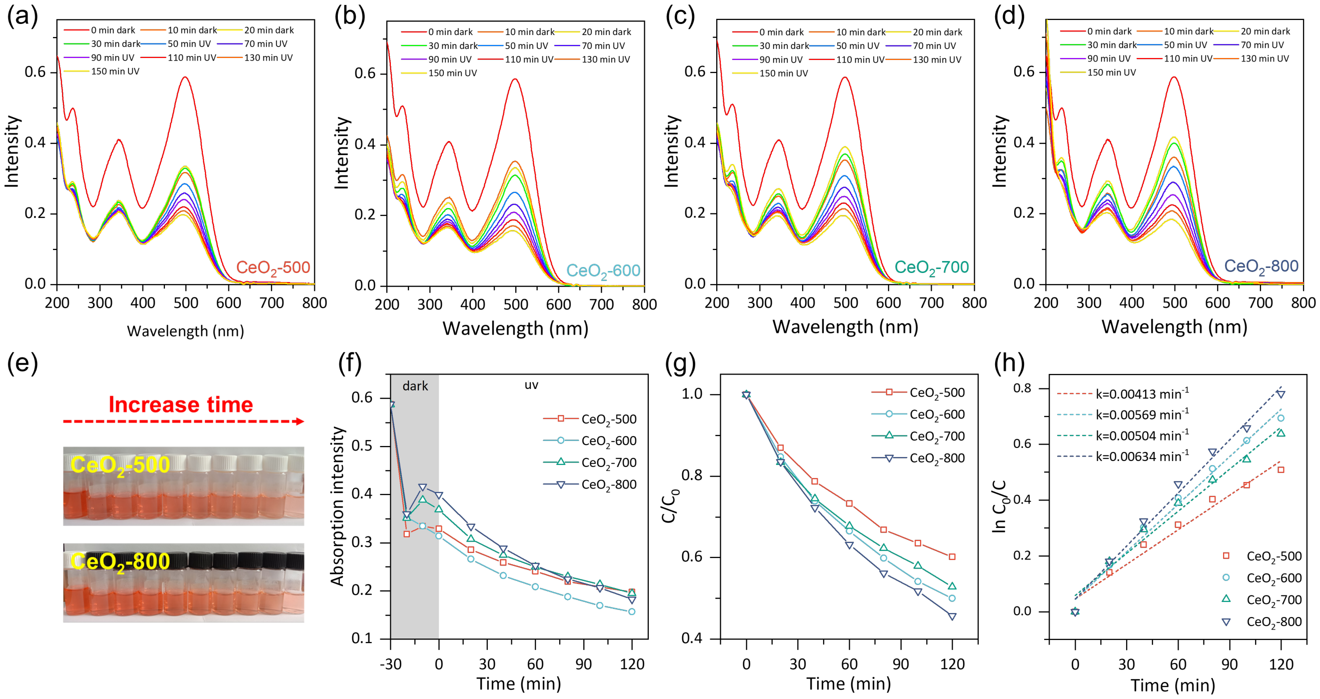

Figure 3. The UV-Vis spectra of the Congo red (CR) dyes with increasing reaction times are shown for (a) CeO_2-500, (b) CeO_2-600, (c) CeO_2-700, and CeO_2-800 samples. Panel (e) presents photograph images of the discoloration of CR solutions after increasing contact time with CeO_2-500 and CeO_2-800. Panel (f) illustrates the changes in CR peak intensity at λ of 498 nm. The (g) C/C_0 and (h) $\ln(C_0/C)$ vs. reaction time are also depicted.

were observed. Upon calcination, the CeO_2 samples exhibit a distinct morphological evolution from well-defined, rod-like structures to increasingly sintered and agglomerated forms. Initially, the uncalcined CeO_2 displays discrete and uniform rods, indicative of a lower temperature synthesis with minimal particle fusion. As the calcination temperature rises, these rods gradually lose their distinctness; they broaden, fuse, and exhibit smoother edges - a transformation signifying increased diffusion and coalescence of particles [34]. At the highest temperatures observed, the rods become almost indistinguishable, with significant agglomeration leading to a bulkier and denser morphology.

Figures 3a to 3d present the UV-Vis spectroscopy spectra of Congo red (CR) solutions with varying contact times for all calcined CeO_2 samples. The CR solutions exhibit maximum absorption at a wavelength of 498 nm, with peak intensities decreasing as contact time increases, indicating a reduction in CR concentration. This trend is consistent across all samples, demonstrating a clear discoloration of the dye upon reaction or contact, which is visually confirmed (Figure 3e). Initially red, the CR solutions progressively lighten upon extended contact with the calcined CeO_2. This also agrees with the UV-Vis spectroscopy investigation previously.

Figure 3f elucidates the concentration changes of the CR solutions over increasing contact times, assessed by the intensity at the peak wavelength of 498 nm. In the absence of light, the CR concentration diminishes to varying extents across the samples, with decreases of over 44%, 46%, 37%, and 32% after 30 minutes of dark contact for CeO_2-500, CeO_2-600, CeO_2-700, and CeO_2-800, respectively. This behavior is attributed to the adsorptive capabilities of CeO_2, as documented in previous literature [35, 36]. Previous studies state that with rising calcination temperatures, which typically reduce the surface area of the materials, the contribution of adsorption decreases [37, 38].

Under UV irradiation, the CR concentration further declines for all samples, showcasing their photocatalytic activity. The CR degradation rate (C/C_0), defined as the ratio of the initial CR concentration (C_0) to the concentration after a certain contact time (C), was calculated to evaluate the photocatalytic behavior of CeO_2 at different calcination temperatures (Figure 3f). The results reveal an accelerated CR concentration reduction for CeO_2-800 compared to the other samples. Specifically, after 120 minutes of UV irradiation, the CR concentration decreased by approximately 39%, 50%, 47%, and 54% for CeO_2-500, CeO_2-600, CeO_2-700, and CeO_2-800, respectively. This increase in photocatalytic performance with higher calcination temperatures is likely due to the enhanced crystallinity of the materials, as indicated by the XRD results [39, 40].

Photocatalytic pseudo-first-order kinetic modeling was employed to further understand the CR degradation by the calcined CeO_2, based on Equation (1):

$$\ln \frac{C_0}{C} = k_t \tag{1}$$

where C_0, (C), (k), and (t) are the CR initial concentration (ppm), CR solution concentration at given time (ppm), the pseudo-first-order constant ($min^{-}1$), and the contact time (min), respectively. The kinetic modeling, displayed in Figure 3g, exhibits a linear correlation with high fitting parameters (R^2 values) of 0.96832, 0.98445, 0.97148, and 0.98586 for CeO_2-500, CeO_2-600, CeO_2-700, and CeO_2-800, respectively. Furthermore, the rate constant k shows an increase with the calcination temperature of the CeO_2, implying an enhanced photocatalytic performance.

4. CONCLUSION

In this study, CeO$_2$ nanostructures were successfully fabricated through a hydrothermal process followed by subsequent calcination at varying temperatures. SEM imaging revealed that all samples maintained a rod-like structure, with crystallite sizes increasing alongside the calcination temperatures. This pattern sharpening and narrowing with elevated temperatures indicate enhanced crystallization and an increase in the size of the CeO$_2$ particles. The photocatalytic capabilities of the calcined CeO$_2$ were assessed through the degradation of Congo red (CR) dye, demonstrating promising potential for wastewater treatment applications. The reduction in CR concentration can be attributed to a combination of adsorption and photocatalytic degradation mechanisms. However, it was observed that higher calcination temperatures somewhat diminish adsorption performance, likely due to alterations in surface charges and a decrease in material surface area. Conversely, the same increase in calcination temperatures correlated with improved photocatalytic activity, which can be ascribed to the higher crystallinity of the materials. These findings highlight the dual role of calcination temperature in modulating both the physical characteristics and functional properties of CeO$_2$ nanostructures. Thus, the optimal calcination temperature for CeO$_2$ nanostructures must balance these effects to maximize their efficacy in environmental applications, particularly in the domain of pollutant degradation in water treatment scenarios.

ACKNOWLEDGEMENTS

This study receives no funding.

AUTHOR CONTRIBUTIONS

AR: Conceptualization, Methodology, Investigation, Writing - Original Draft, Writing - Review & Editing, Visualization, Supervision, Funding acquisition. **RN:** Investigation. **RA:** Resources. **NIK:** Resources, Formal analysis. **KT:** Resources. **TT:** Conceptualization, Methodology, Writing - Original Draft, Writing - Review & Editing, Visualization, Funding acquisition. All authors approved the final manuscript.

REFERENCES

[1] A. Ahmadi, M. Hajilou, S. Zavari, S. Yaghmaei, A comparative review on adsorption and photocatalytic degradation of classified dyes with metal/non-metal-based modification of graphitic carbon nitride nanocomposites: Synthesis, mechanism, and affecting parameters, Journal of Cleaner Production 382 (2023) 134967. https://doi.org/10.1016/j.jclepro.2022.134967.

[2] M. F. Lanjwani, M. Tuzen, M. Y. Khuhawar, T. A. Saleh, Trends in photocatalytic degradation of organic dye pollutants using nanoparticles: A review, Inorganic Chemistry Communications 159 (2024) 111613. https://doi.org/10.1016/j.inoche.2023.111613.

[3] V. Gadore, S. R. Mishra, M. Ahmaruzzaman, Metal sulphides and their heterojunctions for photocatalytic degradation of organic dyes-A comprehensive review, Environmental Science and Pollution Research 30 (39) (2023) 90410–90457. https://doi.org/10.1007/s11356-023-28753-w.

[4] T. Taher, Z. Yu, E. K. A. Melati, A. Munandar, R. Aflaha, K. Triyana, Y. G. Wibowo, K. Khairurrijal, A. Lesbani, A. Rianjanu, Enabling dual-functionality material for effective anionic and cationic dye removal by using Nb2O5/MgAl-LDH nanocomposites, Journal of Hazardous Materials Letters 5 (2024) 100103. https://doi.org/10.1016/j.hazl.2024.100103.

[5] F. T. Geldasa, M. A. Kebede, M. W. Shura, F. G. Hone, Experimental and computational study of metal oxide nanoparticles for the photocatalytic degradation of organic pollutants: a review, RSC Advances 13 (27) (2023) 18404–18442. https://doi.org/10.1039/D3RA01505J.

[6] A. Krishnan, A. Swarnalal, D. Das, M. Krishnan, V. S. Saji, S. Shibli, A review on transition metal oxides based photocatalysts for degradation of synthetic organic pollutants, Journal of Environmental Sciences 139 (2024) 389–417. https://doi.org/10.1016/j.jes.2023.02.051.

[7] S. Yadav, K. Shakya, A. Gupta, D. Singh, A. R. Chandran, A. Varayil Aanappalli, K. Goyal, N. Rani, K. Saini, A review on degradation of organic dyes by using metal oxide semiconductors, Environmental Science and Pollution Research 30 (28) (2022) 71912–71932. https://doi.org/10.1007/s11356-022-20818-6.

[8] A. Rianjanu, K. D. P. Marpaung, E. K. A. Melati, R. Aflaha, Y. G. Wibowo, I. P. Mahendra, N. Yulianto, J. Widakdo, K. Triyana, H. S. Wasisto, T. Taher, Integrated adsorption and photocatalytic removal of methylene blue dye from aqueous solution by hierarchical Nb2O5@PAN/PVDF/ANO composite nanofibers, Nano Materials Science (2023) S2589965123000673https://doi.org/10.1016/j.nanoms.2023.10.006.

[9] T. Wu, R.-t. Guo, C.-f. Li, W.-g. Pan, Recent progress of CeO2-based catalysts with special morphologies applied in air pollutants abatement: A review, Journal of Environmental Chemical Engineering 11 (1) (2023) 109136. https://doi.org/10.1016/j.jece.2022.109136.

[10] S.-Y. Ahn, W.-J. Jang, J.-O. Shim, B.-H. Jeon, H.-S. Roh, CeO$_2$-based oxygen storage capacity materials in environmental and energy catalysis for carbon neutrality: extended application and key catalytic properties, Catalysis Reviews (2023) 1–84https://doi.org/10.1080/01614940.2022.2162677.

[11] T. Montini, M. Melchionna, M. Monai, P. Fornasiero, Fundamentals and Catalytic Applications of CeO$_2$-Based Materials, Chemical Reviews 116 (10) (2016) 5987–6041. https://doi.org/10.1021/acs.chemrev.5b00603.

[12] C. Yang, Y. Lu, L. Zhang, Z. Kong, T. Yang, L. Tao, Y. Zou, S. Wang, Defect Engineering on CeO$_2$-Based Catalysts for Heterogeneous Catalytic Applications, Small Structures 2 (12) (2021) 2100058. https://doi.org/10.1002/sstr.202100058.

[13] M. Panahi-Kalamuei, S. Alizadeh, M. Mousavi-Kamazani, M. Salavati-Niasari, Synthesis and characterization of CeO 2 nanoparticles via hydrothermal route, Journal of Industrial and Engineering Chemistry 21 (2015) 1301–1305. https://doi.org/10.1016/j.jiec.2014.05.046.

[14] M. Lin, Z. Y. Fu, H. R. Tan, J. P. Y. Tan, S. C. Ng, E. Teo, Hydrothermal Synthesis of CeO$_2$ Nanocrystals: Ostwald Ripening or Oriented Attachment?, Crystal Growth & Design 12 (6) (2012) 3296–3303. https://doi.org/10.1021/cg300421x.

[15] A. Rianjanu, A. S. P. Mustamin, E. K. A. Melati, R. Aflaha, N. I. Khamidy, M. Utami, K. Khairurrijal, K. Triyana, F. F. Abdi, H. S. Wasisto, T. Taher, Photocatalytic degradation of aqueous Congo red dye pollutants by rare-earth metal oxide (CeO2) nanorods, Colloids and Surfaces A: Physicochemical and Engineering Aspects 682 (2024) 132919. https://doi.org/10.1016/j.colsurfa.2023.132919.

[16] X. Yang, Y. Liu, J. Li, Y. Zhang, Effects of calcination temperature on morphology and structure of CeO2 nanofibers and their photocatalytic activity, Materials Letters 241 (2019) 76–79. https://doi.org/10.1016/j.matlet.2019.01.006.

[17] T. Velempini, E. Prabakaran, K. Pillay, Recent developments in the use of metal oxides for photocatalytic degradation of pharmaceutical pollutants in water—a review, Materials Today Chemistry 19 (2021) 100380. https://doi.org/10.1016/j.mtchem.2020.100380.

[18] Y. Ren, Z. Ma, P. G. Bruce, Ordered mesoporous metal oxides: synthesis and applications, Chemical Society Reviews 41 (14) (2012) 4909. https://doi.org/10.1039/c2cs35086f.

[19] S. W. Choi, J. Kim, Facile Room-Temperature Synthesis of Cerium Carbonate and Cerium Oxide Nano- and Microparticles Using 1,1Carbonyldiimidazole and Imidazole in a Nonaqueous Solvent, ACS Omega 6 (40) (2021) 26477–26488. https:

//doi.org/10.1021/acsomega.1c03700.

[20] S. K. Meher, G. Ranga Rao, Tuning, via Counter Anions, the Morphology and Catalytic Activity of CeO2 Prepared under Mild Conditions, Journal of Colloid and Interface Science 373 (1) (2012) 46–56. https://doi.org/10.1016/j.jcis.2011.09.050.

[21] A. O. Santos, L. D. Martins, J. H. S. Mezavila, J. D. Serna, N. R. Checca, A. V. Soares, C. M. Fernandes, E. A. Ponzio, J. C. M. Silva, O. C. Alves, Temperature dependence of ferromagnetic behavior in ceria nanoparticles with cubic morphology, Journal of Alloys and Compounds 965 (2023) 171300. https://doi.org/10.1016/j.jallcom.2023.171300.

[22] A. Dos Santos, T. Dantas, J. Costa, L. Souza, J. Soares, V. Caldeira, A. Araújo, A. Santos, Formation of CeO2 nanotubes through different conditions of hydrothermal synthesis, Surfaces and Interfaces 21 (2020) 100746. https://doi.org/10.1016/j.surfin.2020.100746.

[23] X. Yang, Y. Liu, J. Li, Y. Zhang, Effects of calcination temperature on morphology and structure of CeO2 nanofibers and their photocatalytic activity, Materials Letters 241 (2019) 76–79. https://doi.org/10.1016/j.matlet.2019.01.006.

[24] H. Li, F. Meng, J. Gong, Z. Fan, R. Qin, Structural, morphological and optical properties of shuttle-like CeO2 synthesized by a facile hydrothermal method, Journal of Alloys and Compounds 722 (2017) 489–498. https://doi.org/10.1016/j.jallcom.2017.06.156.

[25] C. Li, M. Cui, Q. Sun, W. Dong, Y. Zheng, K. Tsukamoto, B. Chen, W. Tang, Nanostructures and optical properties of hydrothermal synthesized CeOHCO3 and calcined CeO2 with PVP assistance, Journal of Alloys and Compounds 504 (2) (2010) 498–502. https://doi.org/10.1016/j.jallcom.2010.05.151.

[26] E. Nurfani, M. P. Ali, A. Rianjanu, L. Nulhakim, M. S. Anrokhi, G. T. Kadja, Effect of solution molarity on the optical and photocatalytic properties of sprayed ZnO film, Materials Chemistry and Physics 309 (2023) 128412. https://doi.org/10.1016/j.matchemphys.2023.128412.

[27] E. Nurfani, L. Antika, M. S. Anrokhi, W. S. Sipahutar, A. Rianjanu, B. A. Wahjoedi, UV sensitivity enhancement in ZnO:Cu films through simple post-annealing treatment, Physica B: Condensed Matter 628 (2022) 413603. https://doi.org/10.1016/j.physb.2021.413603.

[28] J. Zheng, Z. Wang, Z. Chen, S. Zuo, Mechanism of CeO2 synthesized by thermal decomposition of Ce-MOF and its performance of benzene catalytic combustion, Journal of Rare Earths 39 (7) (2021) 790–796. https://doi.org/10.1016/j.jre.2020.08.009.

[29] A. A. Sery, W. A. Mohamed, F. Hammad, M. M. Khalil, H. Farag, Synthesis of pure and doped SnO2 and NiO nanoparticles and evaluation of their photocatalytic activity, Materials Chemistry and Physics 275 (2022) 125190. https://doi.org/10.1016/j.matchemphys.2021.125190.

[30] T. Taher, S. Maulana, N. Mawaddah, A. Munandar, A. Rianjanu, A. Lesbani, Low-temperature hydrothermal carbonization of activated carbon microsphere derived from microcrystalline cellulose as carbon dioxide (CO2) adsorbent, Materials Today Sustainability 23 (2023) 100464. https://doi.org/10.1016/j.mtsust.2023.100464.

[31] E. Pradeepa, Y. A. Nayaka, Cerium oxide nanoparticles via gel-combustion for electrochemical investigation of pantoprazole in the presence of epinephrine, Journal of Materials Science: Materials in Electronics 33 (23) (2022) 18374–18388. https://doi.org/10.1007/s10854-022-08692-x.

[32] R. Rao, P. Jin, Y. Huang, C. Hu, X. Dong, Y. Tang, F. Wang, F. Luo, S. Fang, A surface control strategy of CeO2 nanocrystals for enhancing adsorption removal of Congo red, Colloid and Interface Science Communications 49 (2022) 100631. https://doi.org/10.1016/j.colcom.2022.100631.

[33] G. Ashok Reddy, H. Shaik, K. N. Kumar, H. D. Shetty, R. I. Jafri, R. Naik, J. Gupta, S. A. Sattar, B. Doreswamy, Synthesis, characterizations, and electrochromic studies of WO3 coated CeO2 nanorod thin films for smart window applications, Physica B: Condensed Matter 647 (2022) 414395. https://doi.org/10.1016/j.physb.2022.414395.

[34] A. El-Shaer, M. Abdelfatah, K. R. Mahmoud, S. Momay, M. Eraky, Correlation between photoluminescence and positron annihilation lifetime spectroscopy to characterize defects in calcined MgO nanoparticles as a first step to explain antibacterial activity, Journal of Alloys and Compounds 817 (2020) 152799. https://doi.org/10.1016/j.jallcom.2019.152799.

[35] C. Hu, X. Hu, R. Li, Y. Xing, MOF derived ZnO/C nanocomposite with enhanced adsorption capacity and photocatalytic performance under sunlight, Journal of Hazardous Materials 385 (2020) 121599. https://doi.org/10.1016/j.jhazmat.2019.121599.

[36] S. J. Olusegun, N. D. Mohallem, Comparative adsorption mechanism of doxycycline and Congo red using synthesized kaolinite supported CoFe2O4 nanoparticles, Environmental Pollution 260 (2020) 114019. https://doi.org/10.1016/j.envpol.2020.114019.

[37] Q. Sun, X. Hu, S. Zheng, J. Zhang, J. Sheng, Effect of calcination on structure and photocatalytic property of N-TiO2/g-C3N4diatomite hybrid photocatalyst for improving reduction of Cr(vi), Environmental Pollution 245 (2019) 53–62. https://doi.org/10.1016/j.envpol.2018.10.121.

[38] P. Nandi, D. Das, Photocatalytic degradation of Rhodamine-B dye by stable ZnO nanostructures with different calcination temperature induced defects, Applied Surface Science 465 (2019) 546–556. https://doi.org/10.1016/j.apsusc.2018.09.193.

[39] S. Jian, Z. Tian, J. Hu, K. Zhang, L. Zhang, G. Duan, W. Yang, S. Jiang, Enhanced visible light photocatalytic efficiency of La-doped ZnO nanofibers via electrospinning-calcination technology, Advanced Powder Materials 1 (2) (2022) 100004. https://doi.org/10.1016/j.apmate.2021.09.004.

[40] A. Sadeghzadeh-Attar, Efficient photocatalytic degradation of methylene blue dye by SnO2 nanotubes synthesized at different calcination temperatures, Solar Energy Materials and Solar Cells 183 (2018) 16–24. https://doi.org/10.1016/j.solmat.2018.03.046.